

Dual mechanisms for transient capacitance anomaly in improper ferroelectrics

Xin Li,^{1‡} Yu Yun,^{1‡} Pratyush Buragohain¹, Haidong Lu¹, Arashdeep Singh Thind^{2,3}, Donald A. Walko⁴, Detian Yang,¹ Rohan Mishra,^{2,3} Alexei Gruverman^{1,5}, Xiaoshan Xu^{1,5*}*

¹Department of Physics and Astronomy, University of Nebraska, Lincoln, Nebraska 68588, USA

²Institute of Materials Science & Engineering, Washington University in St. Louis, St. Louis MO, USA

³Department of Mechanical Engineering & Materials Science, Washington University in St. Louis, St. Louis MO, USA

⁴Advanced Photon Source, Argonne National Laboratory, Argonne, Illinois 60439, USA

⁵Nebraska Center for Materials and Nanoscience, University of Nebraska, Lincoln, Nebraska 68588, USA

‡These authors contributed equally to this work.

*Corresponding author: Xiaoshan Xu (X.X.), Yu Yun (Y.Y.)

Abstract:

Negative capacitance (NC) effects in ferroelectrics can potentially break fundamental limits of power dissipation known as ‘Boltzmann tyranny’. However, the origin of transient NC of ferroelectrics, which is attributed to two different mechanisms involving free-energy landscape and nucleation, is under intense debate. Here, we report coexistence of transient NC and an “S”-shape anomaly during the switching of ferroelectric hexagonal ferrites capacitor in an RC circuit. The early-stage NC arises from the nucleation process, while the late-stage “S”-shape anomaly corresponds to a nascent NC associated with the free-energy landscape. The entire waveform can be reproduced using a hybrid model that simultaneously incorporates these two mechanisms. These results highlight the multi-variable free-energy landscape of hexagonal ferrites that enables abrupt change of internal field and demonstrate that the two mechanisms are not mutually exclusive, resolving the long-standing debate. The behavior of the “S” shape anomaly also provides a pathway to extract parameters of free-energy landscape and switching dynamics.

Ferroelectricity, originating from broken inversion symmetry of crystal structures, can be described using the polarization-dependent free-energy landscape in the phenomenological Landau theory. Spontaneous polarization states locate at energy minima (**Fig. 1(a)**) and the transition from ferroelectric to paraelectric phases corresponds to disappearance of these minima¹⁻⁴. Intriguingly, the barriers between the energy minima can be exploited to boost the capacitance of ferroelectric/dielectric heterostructures, which is promising for enhancing the energy efficiency beyond the lower limit of power consumption in field-effect transistors⁵.

In principle, free-energy landscape of ferroelectrics can be revealed by polarization switching processes⁶⁻¹¹, provided that polarization can be varied continuously. In this case, according to the Landau-Khalatnikov (LK) model^{10,11}, the energy barriers lead to a non-monotonic polarization switching speed and NC response (Section S1 within the Supplemental Material). Naturally, the recent observation of transient NC^{12,13} has been attributed to the mechanism of free-energy landscape. However, LK model is unable to reproduce the transient NC quantitatively, even with multi-grain model¹⁴ or time-dependent viscosity coefficient¹⁵. Moreover, polarization switching is known to normally involve complex processes like nucleation of reversed domains and domain-wall propagation¹⁶⁻¹⁸. Overcoming the nucleation energy barrier can also result in a non-monotonic polarization switching speed (**Fig. 1(b)**) and NC response (Section S2 within the Supplemental Material). Consequently, whether the transient NC originates from the mechanism of free-energy landscape^{12,13,15,19} or the mechanism of nucleation remain under debate.

To resolve this debate, the ferroelectrics with both abrupt change of internal field from LK model (E_{LK} in Fig.1(a)) and nucleation-involved polarization switching are necessary, so that resultant responses of transient capacitance with different origins can compare directly. Here, we focus on improper ferroelectrics hexagonal ferrites (h-RFeO₃, R : rare earth), the crystal structure of h-RFeO₃ consist of triangular lattice of FeO₅ bipyramids sandwiched by rare earth layers (**Fig. 1(c)**). Spontaneous polarization is induced by non-polar K₃ structural distortion²⁰⁻²⁵, characterized by the in-plane displacement of apical oxygen described by the magnitude (Q) and angle (or phase) (ϕ) (**Fig. 1(c)**). With three variables, Q , ϕ , and polarization (P), a complex free-energy landscape is expected²⁶. A two-dimensional (Q and ϕ) representation of this landscape, after minimization with respect to P , is displayed in **Fig. 1(d)**, where three minima at $\phi = 2n\frac{\pi}{3}$ and three at $\phi = (2n + 1)\frac{\pi}{3}$ correspond to $P > 0$ and $P < 0$, respectively, n is an integer²⁷. Notably, the system maintains a constant ϕ during the polarization switching [see **Fig. 1(e)**] before the local energy minimum disappears, at which point a rapid change of E_{LK} is expected, potentially leading to a more obvious NC from the mechanism of free-energy landscape²⁸.

In this work, we demonstrate that two NC mechanisms coexist and manifest in different timescale during the switching process of a hexagonal ferrite ferroelectric capacitor in a RC circuit. The mechanism of nucleation leads to a transient NC with the time scale of nucleation ($\sim 1 \mu\text{s}$), while the mechanism of energy landscape leads to an ‘‘S’’-shape anomaly with a much larger time scale ($\sim 10 \mu\text{s}$) determined by the strength of the internal field. Analysis of the ‘‘S’’-shape anomaly reveals the key parameters of the energy landscape and the switching dynamics.

Epitaxial heterostructures h-YbFeO₃/CoFe₂O₄ (CFO)/La_{0.7}Sr_{0.33}MnO₃ (LSMO) were grown on SrTiO₃ (STO) (111) substrate by pulsed laser deposition. The CFO layer is to buffer the lattice mismatch between h-YbFeO₃ and LSMO bottom electrode^{23,24}; its impact as dielectric layer on improper ferroelectricity can be minimized when h-YbFeO₃ is thick enough²³. In this study, we keep the thickness of the CFO and LSMO layers at 10 nm and 30 nm, respectively. X-ray diffraction (XRD) $\theta - 2\theta$ scan, reflection high energy electron diffraction (RHEED), and high-angle annular dark field (HAADF) STEM confirm the $P6_3cm$ structure of h-YbFeO₃. (Section S3 within the Supplemental Material) The piezoresponse force microscopy (PFM) measurements on bare surface and the polarization-voltage (P - V) hysteresis loops measured using the PUND (positive up and negative down) method demonstrates the switchable spontaneous polarization (Section S3 within the Supplemental Material) .

The polarization switching of h-YbFeO₃ is measured using a RC circuit with a square wave of source voltage (V_S) (**Fig. 2(a)**). Here the resistor limits the currents and polarization switching speed, potentially allowing the ferroelectrics to gradually traverse the energy landscape. **Fig. 2(b)** shows the waveform of V_S and V_{FE} which is the voltage on the ferroelectric capacitor. In contrast to the normal charging process of capacitor in which dV/dt constantly decreases and remains positive, two anomalous features of dV_{FE}/dt can be identified here (**Fig. 2(b)**). The first anomaly occurs in the early stage of $\sim 1 \mu s$ time scale. As shown in **Fig. 2(b)** inset, V_{FE} waveform is non-monotonic with a segment of $dV_{FE}/dt < 0$. Since the current $I = (V_S - V_{FE})/R$ is always positive for $V_S > 0$, one has $dq/dt = I > 0$, where R is the resistance of the resistor in **Fig. 2(a)**. Hence, $dV_{FE}/dt < 0$ corresponds to a dynamic NC due to $dq/dV_{FE} = (dq/dt)/(dV_{FE}/dt) < 0$. The second anomaly appears at a later stage of $\sim 10 \mu s$ time scale. Here dV_{FE}/dt remains positive but exhibits a minimum and a subsequent maximum, as shown in **Fig. 2(c)**, as expected by the LK model¹⁵ (Section S1.3 within the Supplemental Material). We call this feature ‘‘S’’-shape anomaly. (Both anomalies are also observed in h-ScFeO₃/LSMO, see Section S4&S5 within the Supplemental Material)

Next, we discuss the relationships between the first anomaly (NC) and the nucleation mechanism. As shown in **Fig. 3(a)**, we have studied the switching dynamics using square-pulse waveform with the h-YbFeO₃ capacitor directly connected to the voltage source²³. In the early stage, the ferroelectric needs to overcome the nucleation energy barrier, which is responsible for a small initial switching speed dP/dt . Near the end of the nucleation stage, $|dP/dt|$ reaches a peak at around $\sim 1 \mu s$ before P saturates at a long time. According to Kirchoff’s rule and the approximation $A dP/dt \approx -dq/dt$ (Section S6 within the Supplemental Material), one has

$$V_{FE} = V_S - IR = V_S + A \frac{dP}{dt} R, \quad (1)$$

where A is the area of the capacitor. Eq. (1) suggests that the $|dP/dt|$ peak causes a dip in V_{FE} (note for switching V_S from negative to positive, $dP/dt < 0$) and the NC, as observed in **Fig. 2(b)** inset. The switching process of the h-YbFeO₃ capacitor can be described within the framework of nucleation-limited switching (NLS) model²⁸ with a distribution of nucleation time t_0^{29-31} . The voltage dependence of characteristic switching time $\log_{10}(t_0)$ and the width of distribution functions w are displayed in **Fig. 3(b)**. The $\sim 1 \mu s$ time scale of matches that of NC observed in **Fig. 2(b)**.

In principle, nucleation time decreases with external voltage, which is consistent with the observation in **Fig. 3(c)**, which shows the V_{FE} early-stage waveform measured with $R = 6 \text{ k}\Omega$ at

different V_S as a two-dimensional image. A V_{FE} dip accompanied by NC is present for all V_S , as indicated by the calculated t_{dip} (black dots). Overall, t_{dip} decreases as V_S increases as expected for nucleation time. The weak dependence of t_{dip} on V_S may have to do with the incomplete switching for smaller V_S that reduces the nucleation time. A circuit model predicts that the current peak (corresponding to V_{FE} dip) caused by nucleation is shifted earlier unless the RC time constant is much larger than t_0 (Fig. S2.2 within the Supplemental Material). This agrees with **Fig. 3(d)**, where t_{dip} increases with $t_{RC} \equiv RC$ and saturates at large t_{RC} values, C is the capacitance of the ferroelectric capacitor. The model also predicts that t_{dip} saturates at $0.61 t_0$ for $t_{RC} \gg t_0$. One can calculate $t_0 = 1.4 \pm 0.1 \mu s$ from **Fig. 3(d)**, which agrees with the results in **Fig. 3(a&b)**.

We then examine the correlation between the ‘‘S’’-shape anomaly and the free-energy landscape mechanism described by the LK model. According to the LK model, the polarization switching is driven by the sum of the internal field $E_{LK} = -\frac{\partial g}{\partial P}|_{E_{FE}=0}$ and the external field $E_{FE} = -\frac{V_{FE}}{t_{FE}}$ as:

$$\frac{dP}{dt} = \rho(E_{LK} + E_{FE}) \quad (2)$$

where g is the Gibbs free energy density and t_{FE} is the thickness of the ferroelectric, ρ is the viscosity coefficient. Combining Eq. (1) and Eq. (2), one finds the direct effect of E_{LK} on dP/dt and V_{FE} :

$$V_{FE} = V_S + \frac{1}{\frac{t_\rho}{t_{RC0}} + 1} (V_S - t_{FE} E_{LK}) \quad (3)$$

$$\frac{dP}{dt} = \frac{\varepsilon_0}{t_\rho + t_{RC0}} (E_{LK} + E_S) \quad (4)$$

where $t_\rho \equiv \frac{\varepsilon_0}{\rho}$ is the timescale related to viscosity, $t_{RC0} \equiv RC_0$, $C_0 \equiv \frac{A\varepsilon_0}{t_{FE}}$, $E_S \equiv -\frac{V_S}{t_F}$. Eq. (3) suggest non-monotonic E_{LK} causes non-monotonic waveform of V_{FE} .

Two implications about polarization switching timescale from Eq. (4) can be verified by the behavior of the observed ‘‘S’’-shape anomaly. Eq. (4) suggests that E_S needs to be large enough to exceed the peak value of E_{LK} (**Fig. 1(a)**) and thus overcome the energy barrier of polarization switching from one minimum to the other. **Fig. 4(a)** shows the dV_{FE}/dt waveform measured with $R = 6 \text{ k}\Omega$ at various V_S as a two-dimensional image. The ‘‘S’’-shape anomaly that features a minimum and a subsequent maximum in dV_{FE}/dt , disappears at a cut-off voltage $V_{Scut} = 2.5 \pm 0.5 \text{ V}$, in contrast to the presence of NC for all voltages in **Fig. 3(c)**. Meanwhile, t_{max} , the time when the maximum of dV_{FE}/dt occurs, which is plotted on top of the image (black dots), appears to diverge at V_{Scut} . In addition, V_{Scut} appears to be independent of R (**Fig. 4(b)**). Indeed, according to Eq. (4), polarization switching timescale diverges when E_S approaches the peak value of E_{LK} and this is independent of R . Hence, the peak value of E_{LK} is found to be approximately $V_{Scut}/t_{FE} \approx (4 \pm 1) \times 10^7 \text{ V/m}$ for h-YbFeO₃ thin films, comparable to the observed coercivity²³. Eq. (4) also suggests that polarization switching timescale is proportional to $t_{RC0} + t_\rho$, which is indeed observed in **Fig. 4(c)**. Hence, t_ρ can be found from the horizontal intercept of the $t_{max}(t_{RC0})$ relation in **Fig. 4(c)**; the results are independent of V_S considering the experimental uncertainty, as shown in **Fig. 4(d)**. Overall,

we found $t_p = 21 \pm 5$ ns, corresponding to $\rho = (4 \pm 1) \times 10^{-4}$ F/(m·s) for h-YbFeO₃, which is of similar order of magnitude to that reported for ferroelectric HfO₂.¹⁵ Analysis assuming proper ferroelectrics indicate that the slope of the $t_{\max}(t_{\text{RC0}})$ relation, or the magnitude of t_{\max} depends on the peak value of E_{LK} (Section S1.3.1 within the Supplemental Material).

Unlike the homogenous switching assumed by the classic LK model, polarization switching is normally inhomogeneous involving local nucleation and domain wall motion. Nevertheless, local polarization switching is still expected to follow the free-energy landscape decorated with the domain wall energy³². Hence, a convolution of the effects of the free-energy landscape and inhomogeneity is expected, which smears the modulation of V_{FE} waveform by E_{LK} described by Eq. (3). As a result, NC response may turn into the ‘‘S’’-shape anomaly or even totally vanish. The shape of $E_{\text{LK}}(P)$ is key for the observation of ‘‘S’’-shape anomaly. Thus, we further discuss the abrupt changes of E_{LK} of the improper ferroelectric hexagonal ferrites, originating from the multi-variable free-energy landscape (Section S6.3 within the Supplemental Material).

Here we adopt a simplified Gibbs free energy density for hexagonal ferrites assuming a constant Q , since the structural distortion has a larger energy scale than that of the electrostatic interactions:

$$g(\phi, P) = g_0 - (a_P \cos 3\phi + E_F)P + \frac{b_P}{2}P^2 - \frac{\varepsilon_0}{2}E_F^2 \quad (5)$$

where g_0 , $a_P > 0$ and $b_P > 0$ are coefficients that only depend on Q , ε_0 is the vacuum permittivity. $g(\phi, P)$ is displayed in **Fig. 4(e)** near two neighboring potential wells at $\phi = 0$ and $\pi/3$ respectively, where $P_0 = \frac{a_P}{b_P}$ is the spontaneous polarization at zero field.

Assuming an initial state of energy minimum with $\phi = 0$ and $P = P_0 > 0$. In step 1 (**Figs. 5(a&b)**), a constant $E_{\text{FE}} < 0$ is applied to reduce P from P_0 . Because $P < P_0$, $E_{\text{LK}} = a_P - b_P P > 0$ resists E_{FE} . In addition, $\phi = 0$ remains a local minimum because $\partial^2 g / \partial \phi^2 = 9a_P P \cos(3\phi) > 0$. In step 2, P becomes negative. $\phi = 0$ becomes a maximum because $\partial^2 g / \partial \phi^2 < 0$, which triggers a sudden change of ϕ . Minimizing g with respect to ϕ results in $g = g_0 - 1/2 b_P P^2 - 1/2 \varepsilon_0 E_{\text{FE}}^2$, corresponding to $E_{\text{LK}} = b_P P < 0$. Here E_{LK} is in the same direction as E_{FE} which accelerates polarization switching. In step 3, the system reaches $\phi = \pi/3$ (global minimum for $E_{\text{FE}} < 0$). Polarization switching adopts a constant ϕ . Here $E_{\text{LK}} = a_P - b_P P$ becomes positive again, which resists the polarization switching. Although the overall trend, i.e., one minimum and one maximum of E_{LK} in **Fig. 4(f)**, is similar to that of proper ferroelectric in **Fig. 1(a)**, the more abrupt change of $E_{\text{LK}}(P)$ in **Fig. 4(f)** may make its effect potentially more distinguishable.

We use a hybrid model to account for the convoluted effects of free-energy landscape and nucleation (inhomogeneity) quantitatively. Starting with the NLS model^{23,29-31} in which $|dP/dt|$ is determined by E_{FE} and the nucleation processes, we replace E_{FE} with $E_{\text{FE}} + E_{\text{LK}}$ so that $|dP/dt|$ is determined by $E_{\text{FE}} + E_{\text{LK}}$ instead, which is the foundation of the LK model described by Eq. (2). Since the essential shapes of E_{LK} in **Fig. 4(f)** and **Fig. 1(a)** are similar, to facilitate the numerical simulation, we borrow the polynomial form of E_{LK} from the proper FE and assume

$$E_{\text{LK,eff}}(P) = -2\alpha P - 4\beta P^3 \quad (6)$$

where α and β are fitting parameters, similar to the Landau coefficients.

As shown in **Fig. 5(a)**, the theoretical fitting replicates the V_{FE} waveform, achieving much higher consistency in whole time range compared with previous work^{12,14,15,33,34}. For the NC region (**Fig. 5(b)**), once V_S changes sign, the nucleation process causes a maximum of $|dP/dt|$ (see **Fig. S6.2**), a minimum in V_{FE} , and the corresponding NC. Noticeably, $V_{LK,eff}$ at this time scale shows a monotonic decrease, which is clearly unrelated to NC, whereas, for the “S” shape region, $V_{LK,eff}$ exhibits non-monotonic shape (**Fig. 5(c)**). By contrast, $|dP/dt|$ (see **Fig. S10**) has an “S” shape, i.e., monotonic but with a minimum and a maximum in the slope, which explains the “S”-shape anomaly in the V_{FE} waveform according to Eq. (1). The shape of $|dP/dt|$ is damped since it is determined by $V_{LK,eff} + V_{FE}$ instead of V_{FE} in the hybrid model.

In summary, the dual mechanisms for transient NC anomaly, including nucleation and free-energy landscape, are identified as the origin of the early-stage transient NC and the later-stage “S”-shape anomaly, respectively, and well fit by a hybrid model, in improper ferroelectric hexagonal ferrites. The discernable manifestation of the free-energy landscape can be attributed to the abrupt change of LK field, inherited from the multi-variable energy landscape. The dependence of the time scale of NC and that of the “S” shape on RC time constant and external field allows extraction of the intrinsic parameters of nucleation, free-energy landscape, and viscosity. These results may settle the long-standing debate on the origin of transient NC and suggest the potential of hexagonal ferrites for practical applications in low-power electronic devices.

Acknowledgment:

This work is primarily supported by the National Science Foundation (NSF), Division of Materials Research (DMR) under Grant No. DMR-1454618. The research is performed in part in the Nebraska Nanoscale Facility: National Nanotechnology Coordinated Infrastructure and the Nebraska Center for Materials and Nanoscience, which are supported by the NSF under Grant No. ECCS- 1542182, and the Nebraska Research Initiative. Work at Washington University is supported by NSF Grant No. DMR-1806147. STEM experiments are conducted at the Center for Nanophase Materials Sciences at Oak Ridge National Laboratory, which is a Department of Energy (DOE) Office of Science User Facility, through a user project. This research used resources of the Advanced Photon Source, a U.S. Department of Energy (DOE) Office of Science user facility operated for the DOE Office of Science by Argonne National Laboratory under Contract No. DE-AC02-06CH11357.

References

1. Landau, L. D. & Lifshitz, E. M. *Electrodynamics of Continuous Media*. (Oxford, 1960).
2. Ong, L.-H., Osman, J. & Tilley, D. R. Landau theory of second-order phase transitions in ferroelectric films. *Phys. Rev. B* 63,144109 (2001).
3. Daraktchiev, M., Catalan, G. & Scott, J. F. Landau Theory of Ferroelectric Domain Walls in Magnetoelectrics. *Ferroelectrics* 375, 122-131 (2008).
4. Kumar, A. & Waghmare, U. V. First-principles free energies and Ginzburg-Landau theory of domains and ferroelectric phase transitions in BaTiO₃. *Phys. Rev. B* 82,054117(2010).
5. Íñiguez, J., Zubko, P., Luk'yanchuk, I. *et al.* Ferroelectric negative capacitance. *Nat Rev Mater* 4, 243–256 (2019)
6. Gruverman. A., Rodriguez. B. J., Dehoff. C. Direct studies of domain switching dynamics in thin film ferroelectric capacitors. *Appl. Phys. Lett.* 87, 082902 (2005).
7. D. J. Jung , M. Dawber , J. F. Scott. *et al.* Switching Dynamics in Ferroelectric Thin Films: An Experimental Survey. *Integrated Ferroelectrics*, 48:1, 59-68 (2002).
8. J. F. Scott. A review of ferroelectric switching. *Ferroelectrics*, 503:1, 117-132(2016).
9. Gruverman. A, Kholkin. A . Nanoscale ferroelectrics: processing, characterization and future trends. *Rep. Prog. Phys.* 69, 2443(2006).
10. Vizdrik. G., Ducharme. S., Fridkin. V. M. *et al.* Kinetics of ferroelectric switching in ultrathin films. *Phys. Rev. B* 68, 094113(2003).
11. Fridkin. V., Levlev. A., Verkhovskaya. K. Switching in One Monolayer of the Ferroelectric Polymer, *Ferroelectrics*, 314:1, 37-40(2005).
12. Khan. A., Chatterjee. K., Wang. B. *et al.* Negative capacitance in a ferroelectric capacitor. *Nature Mater* 14, 182–186 (2015).
13. Hoffmann, M., Fengler, F.P.G., Herzig, M. *et al.* Unveiling the double-well energy landscape in a ferroelectric layer. *Nature* 565, 464–467 (2019).
14. Hoffmann, M., Pešić, M., Chatterjee, K., Khan, A. I., Salahuddin, S., Slesazeck, S., Schroeder, Uwe., Mikolajick, T. Direct Observation of Negative Capacitance in Polycrystalline Ferroelectric HfO₂. *Adv. Funct. Mater.* 26, 8643–8649 (2016).

15. Chang, S.-C., Avci, U. E., Nikonov, D. E. Physical Origin of Transient Negative Capacitance in a Ferroelectric Capacitor. *Phys. Rev. Applied* 9, 014010 (2018).
16. Yang, T. J., Gopalan, V., Swart, P. J. et al. Direct Observation of Pinning and Bowing of a Single Ferroelectric Domain Wall. *Phys. Rev. Lett.* 82, 4106 (1999).
17. Shin, Y.H., Grinberg, I., Chen, I.W. et al. Nucleation and growth mechanism of ferroelectric domain-wall motion. *Nature* 449, 881–884 (2007).
18. Grigoriev, A., Do, D.H., Kim, D. M. et al. Nanosecond Domain Wall Dynamics in Ferroelectric $\text{Pb}(\text{Zr},\text{Ti})\text{O}_3$ Thin Films. *Phys. Rev. Lett.* 96, 187601 (2006).
19. Catalan, G., Jiménez, D., Gruverman, A. Negative capacitance detected. *Nature Mater* 14, 137–139 (2015).
20. Wang, W. et al. Room-temperature multiferroic hexagonal LuFeO_3 films. *Phys. Rev. Lett.* 110, 237601 (2013).
21. Xu, X. & Wang, W. Multiferroic hexagonal ferrites (h-RFeO_3 , $\text{R} = \text{Y}, \text{Dy-Lu}$): a brief experimental review. *Mod. Phys. Lett. B* 28, 1430008 (2014).
22. Sinha, K. et al. Tuning the Neel Temperature of Hexagonal Ferrites by Structural Distortion. *Phys. Rev. Lett.* 121, 237203 (2018).
23. Yun, Y. et al. Spontaneous Polarization in an Ultrathin Improper-Ferroelectric/Dielectric Bilayer in a Capacitor Structure at Cryogenic Temperatures. *Phys. Rev. Appl.* 18 (2022).
24. Li, X., Yun, Y., Thind, A.S. et al. Domain-wall magnetoelectric coupling in multiferroic hexagonal YbFeO_3 films. *Sci Rep* 13, 1755 (2023).
25. Li, X., Yun, Y., Xu, X. S. Improper ferroelectricity in ultrathin hexagonal ferrites films. *Appl. Phys. Lett.* 122, 182901 (2023)
26. Artyukhin, S., Delaney, K. T., Spaldin, N. A. & Mostovoy, M. Landau theory of topological defects in multiferroic hexagonal manganites. *Nature Mater.* 13, 42–49 (2014).
27. Zhang, C. X., Yang, K. L., Jia, P. et al. Effects of temperature and electric field on order parameters in ferroelectric hexagonal manganites. *J. Appl. Phys.* 123, 094102 (2018).
28. Hoffmann, M., Slesazeck, S., Schroeder, U. et al. What's next for negative capacitance electronics?. *Nat Electron* 3, 504–506 (2020).

29. Tagantsev, A. K., Stolichnov, I., Setter, N., Cross, J. S. & Tsukada, M. Non-Kolmogorov-Avrami switching kinetics in ferroelectric thin films. *Phys. Rev. B* 66, 214109 (2002).
30. Jo, J. Y., Han, H. S., Yoon, J.-G. Domain Switching Kinetics in Disordered Ferroelectric Thin Films. *Phys. Rev. Lett.* 99, 267602 (2007).
31. Gruverman, A., Wu, D., and J. F. Scott. Piezoresponse Force Microscopy Studies of Switching Behavior of Ferroelectric Capacitors on a 100-ns Time Scale. *Phys. Rev. Lett.* 100, 097601(2008).
32. Yoshihiro Ishibashi. A Model of Polarization Reversal in Ferroelectrics. *J. Phys. Soc. Japan* 59 4148 (1990).
33. Kim, Y. J., Park, H. W., Hyun, S. D. et al. Voltage Drop in a Ferroelectric Single Layer Capacitor by Retarded Domain Nucleation. *Nano Lett* 17, 7796-7802(2017).
34. Hao, Y., Li, T., Yun, Y. et al. Tuning Negative Capacitance in $\text{PbZr}_{0.2}\text{Ti}_{0.8}\text{O}_3/\text{SrTiO}_3$ Heterostructures via Layer Thickness Ratio. *Phys. Rev. Applied* 16, 034004(2021).

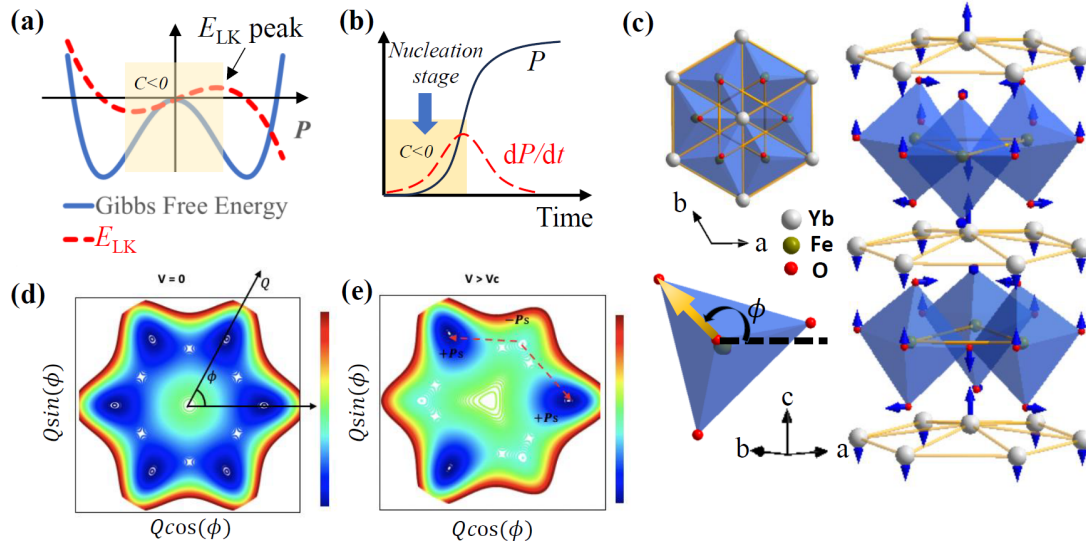


Fig. 1 (a) Schematics of free-energy landscape and internal field E_{LK} as well as the NC region for proper ferroelectrics. (b). Time-dependent polarization and the NC region for a nucleation process. (c) Atomic structure of h-YbFeO₃. The arrows indicate the displacement pattern of the K₃ distortion mode. (d) The free-energy landscape of improper ferroelectric h-RFeO₃ with (d) zero and (e) positive external field.

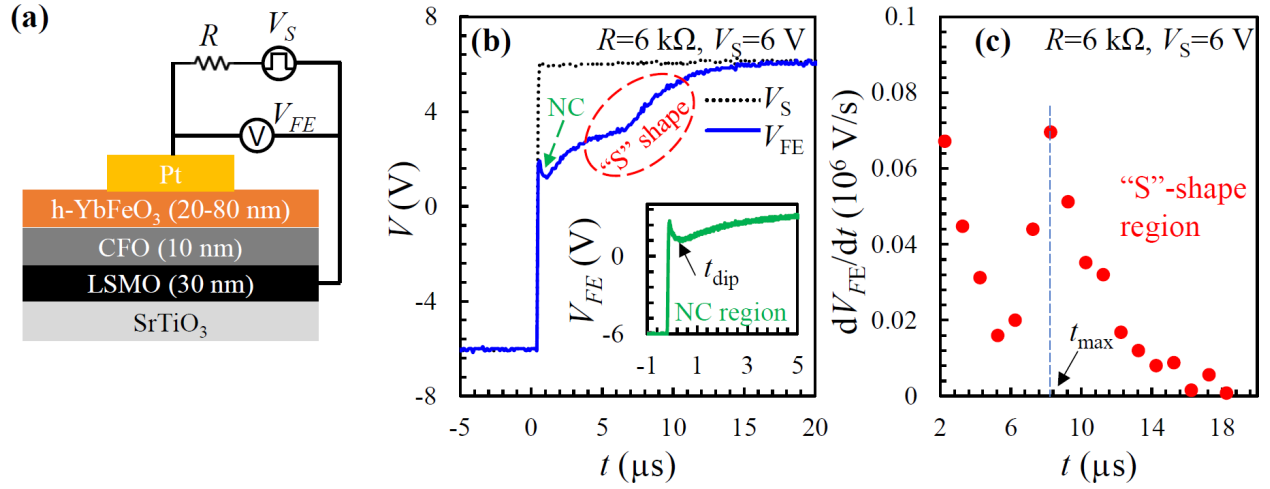


Fig. 2 (a) Schematic diagram of experimental setup. V_{FE} (b) and dV_{FE}/dt (c) waveform measured with $R=6\text{ k}\Omega$ and $V_S=6\text{ V}$. The sparse data points of dV_{FE}/dt in (c) is the result of large bin size of the V_{FE} data chosen to calculate the derivative. The thickness of h-YbFeO₃ is 60 nm.

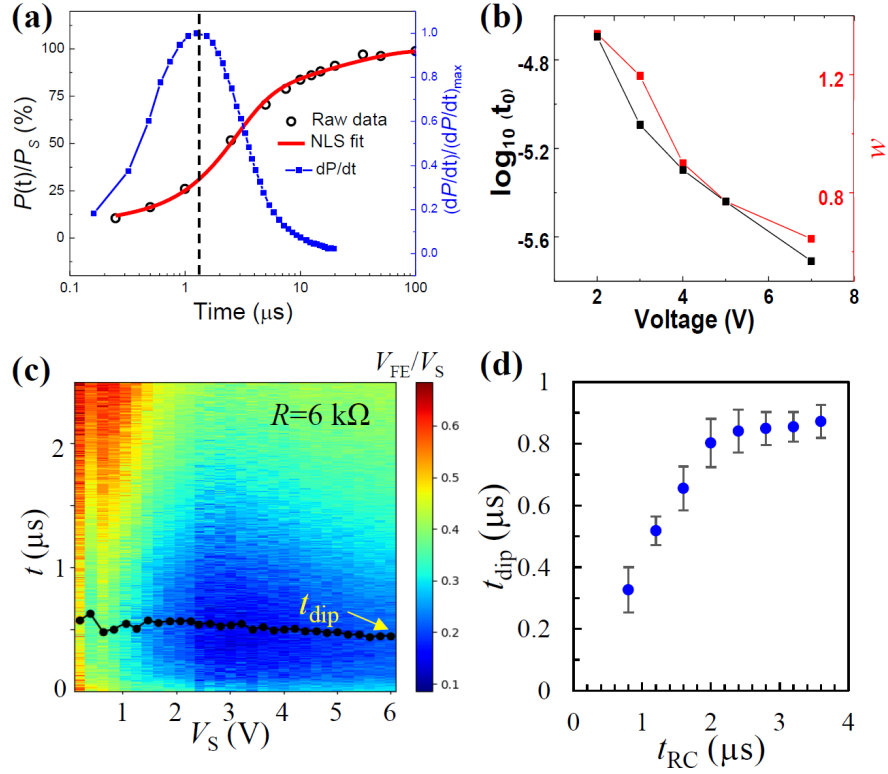


Fig. 3 (a) Time-dependent polarization switching and related fitting by the NLS model, with data from Ref. 23. (b) Dependence of nucleation time t_0 and distribution width w on the applied voltage. (c) V_{FE} waveform measured with $R=6\text{ k}\Omega$ at different V_S . The dots indicate the time t_{dip} where the minimum occurs. (d) Dependence of t_{dip} on t_{RC} where $C \approx 0.2\text{ nF}$. For each t_{RC} (or R) value, the t_{dip} value and error bar are calculated from the average and standard deviation of the values measured with different V_S respectively. The thickness of h-YbFeO₃ is 31 nm for (a) and (b) and 60 nm for (c) and (d).

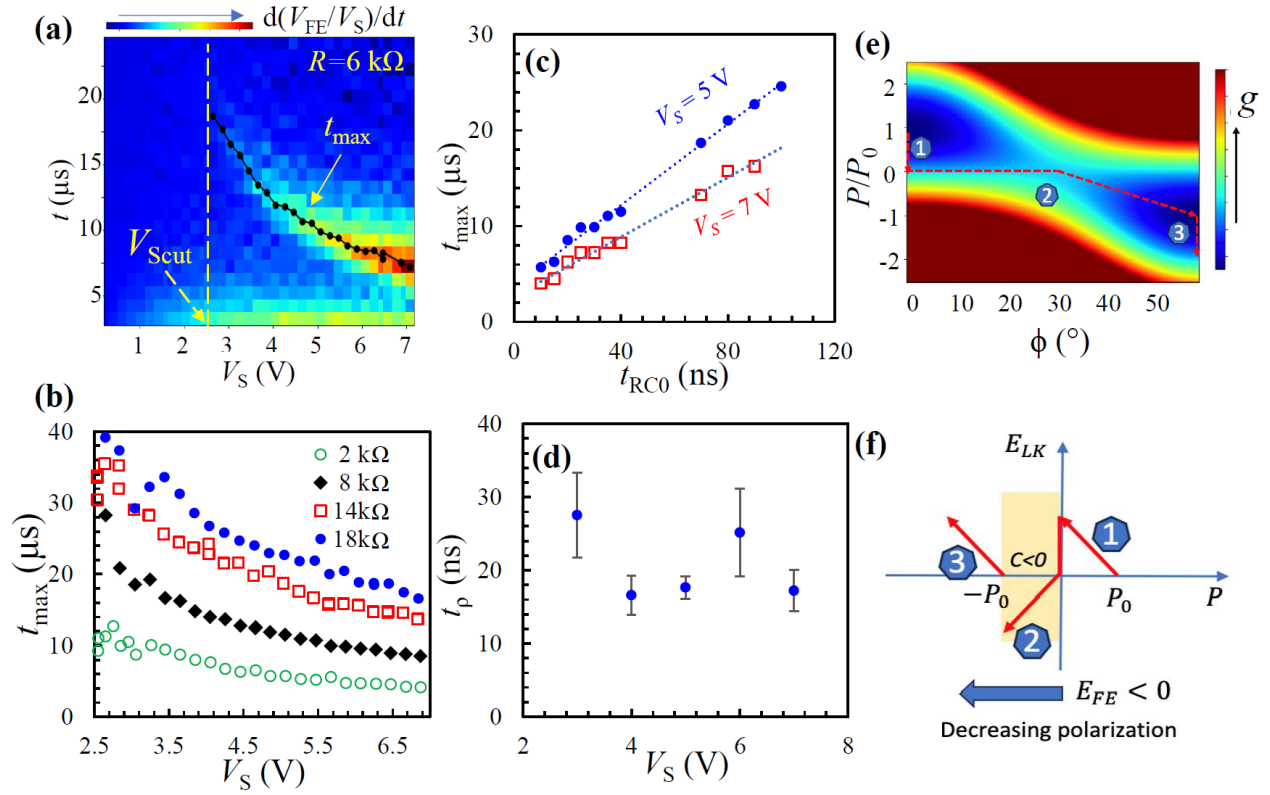


Fig. 4 (a) dV_{FE}/dt waveform measured with $R=6$ k Ω at different V_S . The dots indicate the time t_{max} where the maximum occurs. Vertical dashed line indicates a cut-off voltage V_{Scut} at which the maximum disappears. (b) Dependence of t_{max} on V_S for different R . (c) Dependence of t_{max} on t_{RC0} where $C_0 \approx 5$ pF. Markers (round and square) and dashed lines are experimental data and linear fit respectively. (d) t_p extracted from (c), see text. Schematic of the polarization switching path (e) and the polarization-dependent E_{LK} (f) from $-P_0$ to $+P_0$ for improper ferroelectric h-RFeO₃. The thickness of h-YbFeO₃ is 60 nm.

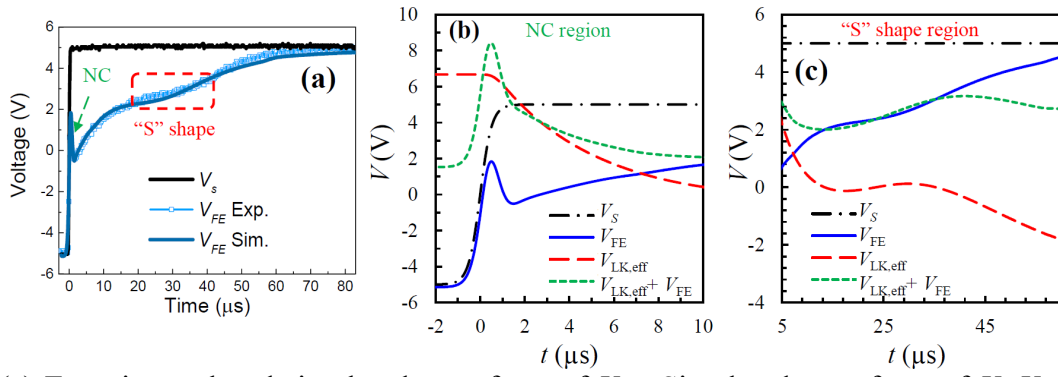


Fig. 5 (a) Experimental and simulated waveform of V_{FE} . Simulated waveform of V_s , V_{FE} , $V_{LK,eff}$, and $V_{FE} + V_{LK,eff}$ in the NC region (b) and the "S" shape region (c). The thickness of h-YbFeO₃ is 60 nm.